



## Quantitative and qualitative investigation into the impact of focused ultrasound with microbubbles on the triggered release of nanoparticles from vasculature in mouse tumors

Chung-Yin Lin <sup>a,b</sup>, Tzu-Ming Liu <sup>a</sup>, Chao-Yu Chen <sup>c</sup>, Yen-Lin Huang <sup>d</sup>, Wei-Kai Huang <sup>c</sup>, Chi-Kuang Sun <sup>e</sup>, Fu-Hsiung Chang <sup>c,\*</sup>, Win-Li Lin <sup>a,b,\*</sup>

<sup>a</sup> Institute of Biomedical Engineering, National Taiwan University, Taipei, Taiwan

<sup>b</sup> Division of Medical Engineering Research, National Health Research Institutes, Miaoli, Taiwan

<sup>c</sup> Institute of Biochemistry and Molecular Biology, National Taiwan University, Taipei, Taiwan

<sup>d</sup> Department of Nephrology, Chang Gung Memorial Hospital, Taoyuan, Taiwan

<sup>e</sup> Department of Electrical Engineering and Graduate Institute of Photonics and Optoelectronics, National Taiwan University, Taipei, Taiwan

### ARTICLE INFO

#### Article history:

Received 24 June 2009

Accepted 27 May 2010

Available online 2 June 2010

#### Keywords:

Focused ultrasound

Microbubbles

Lipid-coated quantum dots

Nanoparticle delivery

Tumor

### ABSTRACT

Ultrasound-mediated microbubble destruction may enhance the release of nanoparticles from vasculature to tumor tissues. In this study, we used four different sizes of lipid-coated CdSe quantum dot (LQD) nanoparticles ranging from 30 to 180 nm, 1.0-MHz pulsed focused ultrasound (FUS) with a peak acoustic pressure of 1.2-MPa, and an ultrasound contrast agent (UCA; SonoVue<sup>®</sup>) at a dose of 30 µL/kg to investigate any enhancement of targeted delivery. Tumor-bearing male Balb/c mice were first injected with UCA intravenously, were then sonicated at the tumors with FUS, and were finally injected with 50 µL of the LQD solution after the sonication. The mice were sacrificed about 24 h after the sonication, and then we quantitatively and qualitatively evaluated the deposition of LQDs in the tumors by using graphite furnace atomic absorption spectrometry (GF-AAS), photoluminescence spectrometry (PL), and harmonic generation microscopy (HGM). Further, immunoblotting analysis served to identify the biochemical markers reflecting the vascular rupture. The experimental results show that the amount of LQDs deposited in tumor tissues was greater in cases of FUS/UCA application, especially for smaller LQDs, being 4.47, 2.27, 0.99, and 0.82 (µg Cd)/(g tumor) for 30, 80, 130, and 180 nm of LQDs, respectively; compared to 1.12, 0.75, 0.26, and 0.34 (µg Cd)/(g tumor) in absence of FUS/UCA. The immunoblotting analysis further indicates that FUS-induced UCA oscillation/destruction results in rupture areas in blood vessels increasing the vascular permeability and thus justifying for the higher quantity of nanoparticles deposited in tumors.

© 2010 Elsevier B.V. All rights reserved.

### 1. Introduction

Tumor vasculature plays a vital role in tumor growth and metastasis. Newly formed tumor vessels stimulate cells' sprouting and branching as is characteristic of a functional vascular network [1]. The tumor vasculature constituting a deficient endothelium and basement membrane is relatively unstable, dilated, tortuous, and chaotic, resulting in the resistance of blood flow to tumors [2]. In addition, high interstitial fluid pressure (IFP) in tumors reduces fluid transportation through the tumor interstitial space [3], and it is a

barrier to effective drug delivery and not favorable for tumor chemotherapy [4,5].

Jain and his colleagues have clearly shown that hyperthermia could lower tumor interstitial pressure in amelanotic melanoma (A-Mel-3) in Syrian golden hamsters [6]. Their investigation supports the assertion that hyperthermia can facilitate the delivery of therapeutic reagents to tumors [7,8], and that this improved delivery reflects the "heating process"-based increase in intravascular pressure, which, in turn, allows more nanoparticles to cross the vascular barrier to tumors with significant diffusion and driving force [7]. Research has examined the use of ultrasound for noninvasively enhancing the delivery of therapeutic reagents into tumors [4]. For overcoming the drug-delivery difficulties posed by vascular barriers, ultrasound can increase vascular-wall permeability and can elevate intracellular uptake [9,10]. Ultrasound has different capabilities for triggering a drug release from a carrier and increases intracellular permeability [11]. One effective use of ultrasound is to provide nonlethal temperature elevation to enhance the delivery of therapeutic reagents to

\* Corresponding author. Lin is to be contacted at Institute of Biomedical Engineering, National Taiwan University, Taipei, 100, Taiwan. Tel.: +886 2 23123456x81445; fax: +886 2 23940049. Chang, Institute of Biochemistry and Molecular Biology, National Taiwan University, Taipei, 100, Taiwan. Tel.: +886 2 23123456x88203; fax: +886 2 23915295.

E-mail addresses: [fchang@ntu.edu.tw](mailto:fchang@ntu.edu.tw) (F.-H. Chang), [winli@ntu.edu.tw](mailto:winli@ntu.edu.tw) (W.-L. Lin).

tumors. Additionally, the injection of an ultrasound contrast agent (UCA) is generally associated with ultrasound sonication for enhancing the effectiveness of nonthermal delivery [11,12]. Through the interaction of tumor vasculature and ultrasound sonication in the presence of UCA, the oscillation and destruction of microbubbles as well as microstreaming and radiation forces may result in the rupture of vascular barriers and increase the tumor's vascular permeability [11,13].

Nanoparticle-based drugs used in biological systems exhibit many benefits for drug delivery, such as higher purity leading to reduced dosages and nanosized properties leading to successful crossing of vascular barriers [14]. These properties allow nanoparticles not only to move through tumor vasculature to the interstitium but also to accumulate in tumor tissues. Subsequently, the properties may also provide specific and effective cellular uptake and permit a prolonged presence of nanoparticles in tumor cells [15]. Currently, numerous nanocarrier-mediated delivery technologies such as various uses of micelles [4,5], dendrimers [16,17], liposomes, polymeric nanoparticles [18], and polysaccharides [19] are being rapidly developed for improvements in tumor-therapy efficacy [20].

In this study, a focus on vasculature rupture was made with focused ultrasound sonication in the presence of UCA and functionalized quantum dot (QD) nanoparticles were used to determine whether or not a nanodrug has been effectively delivered to tumors. QDs have optical properties typical of surrogate markers and hence do not need the addition of a molecular tag to enable *in vivo* monitoring [21–23]. The enhanced permeation and retention of tumor properties can be exploited for the passive targeting delivery of QDs and for, in turn, the elevation of accumulation in the tumor tissue [24]. In order to reduce cytotoxicity and increase bioavailability [25,26], QDs coated with lipids were used in this study. The approach of using lipid-coated QDs (LQDs) in combination with optical imaging and nanomedical carriers would make it possible to detect tumors with molecular imaging [25]. LQDs served as surrogate markers to detect and track the tumor cells *in vivo* with manifest brightness and high resolution under harmonic generation microscopy (HGM) [27]. HGM was used to obtain microscopic evidence regarding the extravascular deposition of nanoparticles in tumors. Without photo-damage and photo-bleaching to the imaged tissues, HGM with LQDs proved to be excellent for cellular imaging when compared to confocal scanning microscopy. Furthermore, the excitation wavelength enabled HGM with LQDs to observe tumor tissues both deeply and noninvasively. Fig. 1 shows the ultrasound-mediated microbubble destruction strategy whose function was to enhance LQD delivery into tumor tissues. A UCA was injected intravenously through the tail vein first, a focused ultrasound (FUS) was immediately sonicated at the tumor, and then LQDs were injected intravenously. Ultrasound sonication would induce the microbubbles oscillation in blood vessels, causing stable or inertial cavitation. The bubble oscillation, the stable cavitation, or the inertial cavitation may induce the rupture of blood vessel walls, resulting in a greater delivery of LQDs into the tumor tissue. We used atomic absorption spectrometry (AAS), photoluminescence spectrometry (PL), and HGM to evaluate quantitatively and qualitatively the different sizes of LQDs deposited in the tumor tissues, and we used immunoblotting analysis to identify the characteristics of the vascular rupture.

## 2. Materials and methods

### 2.1. Materials

The lipids for encapsulating fluorescent QDs were 1,2-Dioleoyl-sn-Glycero-3-Phosphoethanolamine-N-[Methoxy(Poly(ethylene glycol)-2000)] (DOPE-PEG2000) and cholesterol, which were purchased from Avanti Polar Lipids (Alabaster, AL). In our laboratory, we synthesized 3-β-[N-(2-guanidinoethyl)carbamoyl]-cholesterol (GEC-

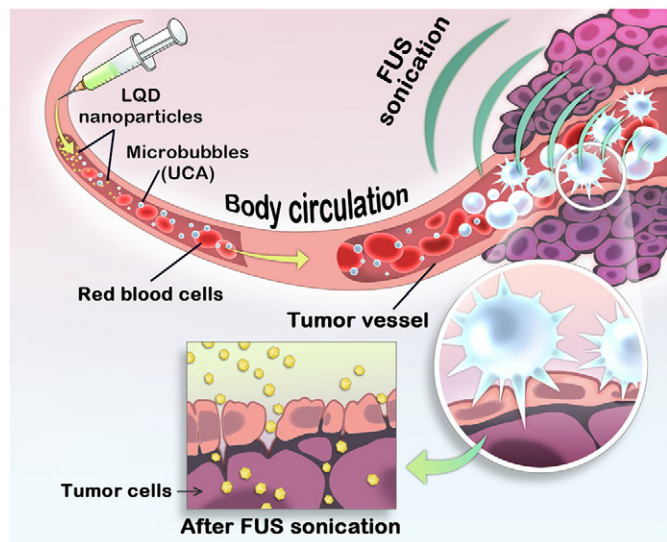


**Fig. 1.** A schematic representation of nanoparticle delivery through tumor microvasculature enhanced by focused ultrasound (FUS) sonication in the presence of microbubbles (ultrasound contrast agent (UCA)). The yellow hexagons represent lipid-coated quantum dot (LQD) nanoparticles, white circles represent microbubbles, and red circles represent red blood cells. Ultrasound-mediated microbubbles' oscillation and cavitation could disrupt tumor vascular walls, and this disruption would enhance the delivery of LQDs to interstitial spaces.

Chol) [28]. These lipids were dissolved in chloroform, sealed in ampoules, filled with argon gas, and stored at  $-20^{\circ}\text{C}$  before use. The anti-mouse P-selectin/CD62P primary antibody and the goat anti-mouse IgG (H+L) HRP-labeled secondary antibody were from R&D Systems (Minneapolis, MN) and AnaSpec Inc. (San Jose, CA), respectively. Super pure nitric acid and Tween 20 were from Merck Biochem. (Darmstadt, Germany). The ultrasound contrast agent (UCA, SonoVue®) was from Bracco Int. (Amsterdam, The Netherlands). Other chemicals, if not specified, were from Aldrich-Sigma (St. Louis, MO).

### 2.2. Synthesis of lipid-coated CdSe quantum dot nanoparticles (LQDs)

The CdSe cores were synthesized according to the standard protocol in which trioctylphosphine oxide (TOPO) served as the stabilizer [28,29], and a UV-Vis spectrometer facilitated the analysis of both the absorption spectrum and the concentration of TOPO-stabilized CdSe quantum dots (QDs). Then, these QDs were precipitated and suspended in chloroform before further functionalization. Lipid-coated CdSe quantum dots (LQDs) were prepared by means of the standard thin-film hydration method [30] and ultrasound sonication. GEC-Chol and cholesterol at the 1:1 molar ratio, and a suitable amount of DOPE-PEG2000 (10% molar ratio for 30 nm; 1% molar ratio for 80 nm; 0.1% molar ratio for 130 and 180 nm) in chloroform, were mixed with hydrophobic CdSe QDs, and were then evaporated under reduced pressure. The resulting LQD film was hydrated in 400  $\mu\text{L}$  of a 5% dextrose solution, yielding the final concentrations of cationic lipids (400  $\mu\text{M}$ ) and of CdSe QDs (500  $\mu\text{g}/\text{mL}$ ). The LQD solution was intensively sonicated by means of an ultrasound Sonicator® (Misonix S3000, New York, NY) at a frequency of 20 kHz, and with 1 W of power for 30 s to form the sizes of 30, 80, and 180 nm of LQDs, and for 45 s to form the 130 nm of LQDs. The solution was then filter-sterilized through a Millex 0.22  $\mu\text{m}$  diameter filter and stored at room temperature before use. A photoluminometer (Perkin Elmer LS55, Waltham, MA) served to measure the fluorescence and emission spectra of LQDs, and transmission electron microscopy (TEM) served to scan their morphology. The particle diameters were

determined by means of a dynamic light-scattering (DLS) particle analyzer (Nano-ZS90, Malvern Instruments, Malvern, Worcestershire, UK). The size of these LQDs ranged from 30 to 180 nm and could be stored in a dextrose solution for more than 3 months in airtight vials without changing their physical properties. The lipids used in this study (GEC-Chol, Chol, and DOPE-PEG2000) can benefit, in several ways, the effort to align LQD nanoparticles with the experimental requirements. First, cholesterol-based derivatives have a high transition temperature for maintaining the stability of LQDs in the biological circulation. Second, the phospholipid layer features parts of DOPE-PEG2000 that can facilitate the water-solubility of LQDs and that can prevent their aggregation in the body's circulation.

### 2.3. Cell culture

Mouse colorectal adenocarcinoma CT-26 cells were from the American Type Culture Collections (ATCC, MD). The CT-26 cells were cultured in the RPMI medium supplemented with 10% fetal bovine serum in a 37 °C, 5% CO<sub>2</sub> incubator for 24 h with complete cell attachment. We determined cell number and viability by using a hemocytometer with trypan blue exclusion test.

### 2.4. In vivo animal model

This study used 62 Balb/c male mice, each being six-week-old and weighing from 18 to 23 g. CT-26 cells were implanted into the hypodermis on the back of each mouse for tumor formation, and the experiment was executed as the tumor grew to 5 mm in diameter. The mice were anesthetized with an intraperitoneal injection of a combination solution of ketamine (30 mg/kg) and acepromazine (0.75 mg/kg). The experimental procedure met the criteria outlined by the Institutional Animal Care and Use Committee of National Taiwan University (NTU-IACUC), and we handled the mice according to the guidelines in The Handbook of the Laboratory Animal Center, National Taiwan University. We performed all experiments as carefully as possible to minimize the suffering of the animals.

### 2.5. Ultrasound system and experimental procedure

A single-element FUS transducer with a frequency of 1.0-MHz, a diameter of 38 mm, and a curvature radius of 63.5 mm (A392S, Panametrics, Waltham, MA) was mounted on the bottom of a removable cone (inner diameters for top and bottom: 12 mm and 38 mm, respectively; cone length: 58 mm) filled with distilled and degassed water. This cone was used to guide the ultrasound beam to the desired region. A polyurethane (PU) membrane covered the tip of the cone firmly so that there were no bubbles in the water. The center of the focal zone was about 5.3 mm away from the cone tip. A function generator (33220A, Agilent, Palo Alto, CA) that was connected with both a power amplifier (150A250A, Amplifier Research, Souderton, PA) and a power meter/sensor module (4421, Bird, Cleveland, OH) drove the FUS transducer. The skin over each tumor was covered with a 5-mm-thick acoustic transmission gel (Pharmaceutical Innovations, Newark, NJ), the cone's tip was immersed in the gel and targeted on the tumor, and then the cone with the FUS transducer was circularly scanned above the tumor with a diameter of 3 mm for sonicating the tumor. To have maximum effect on the tumor's vascular permeability for nanoparticles, we arranged the focal zone of the FUS transducer in the tumor in this study. The acoustic pressure at the focal point was 1.2-MPa, measured with a needle hydrophone (HPM1/1, Precision Acoustics LTD, Dorchester, UK).

Pulsed FUS sonifications were applied with a 10-ms burst length, a 1% duty cycle, a 1 Hz pulse repetition frequency, and a 2-min-sonication duration. An ultrasound contrast agent (UCA, SonoVue®; phospholipid-coated microbubbles, mean diameter: about 2.5 μm, and microbubble concentration: 2–5 × 10<sup>8</sup> bubbles/mL) was intrave-

nously injected at a dose of 30 μL/kg through the tail vein, and 50 μL of the injection of LQD solution was injected. In the *in vivo* experiment, five groups were studied: the control group, the LQD group (LQD injection only), the UCA + LQD group (UCA injection, followed by LQD injection), the FUS + LQD group (FUS sonication, followed by LQD injection), and the UCA + FUS + LQD group (UCA injection, followed by FUS sonication, and then LQD injection). All the mice were sacrificed about 24 h after LQD injection for the accumulation of LQD nanoparticles in the tumors. Tumor tissues were then assembled for cadmium accumulation determination, a photoluminescence (PL) scan, and harmonic generation microscopy (HGM) imaging [28]. The tissues were frozen in liquid nitrogen and kept at –80 °C for later use.

### 2.6. Quantitative determination of cadmium accumulation in tumor tissue with graphite furnace atomic absorption spectrometry (GF-AAS)

An atomic absorption spectrometry (SpectrAA-220FS, Varian Inc., Palo Alto, CA), equipped with cadmium hollow cathode lamps, served to identify the cadmium accumulation in the tumor tissue. The 228.8 nm wavelength and the Air–Argon flame were set up according to instrument guidelines. A cadmium ICP standard solution (National Institute of Standards and Technology, Gaithersburg, MD) was prepared for calibrating the standard curve of a 0–10 μg/L concentration. A tumor tissue sample of 100 mg was located in a 1.5 mL digestion tube with 0.5 mL super pure nitric acid (Suprapur®, 65%, 1.39 g/mL) added to the tube. The sample solution was for analyzing the cadmium concentration of LQDs with GF-AAS, and the tissue sampling was repeated three times in the analysis.

### 2.7. Qualitative analysis of LQDs with photoluminescence spectrometry (PL)

Tumor tissues were prepared and sectioned according to standard procedures. The tissues were removed from an –80 °C freezer to a –20 °C Leica CM3050 S Cryostat (Meyer Inc., TX). Then, the tissue was blocked by a Tissue-Tek OCT compound (Sakura Finetek Inc., CA) and was cut into 15 μm sections on SuperFrost® glass slides (Thermo Fisher Scientific, Braunschweig, Germany). The tissue sections were scanned for their PL spectra with a Hitachi F4500 Fluorescence Spectrometer (Hitachi High-technologies, Tokyo, Japan). The instrument-operating parameters were PMT voltage 700 V, emission wavelength 410 nm, and emission slit 1 or 2.5 nm. The intensity of the fluorescence observed could be adjusted via the width of the emission slit.

### 2.8. Deposition analysis of LQDs with optical harmonic generation microscopy (HGM)

The tumor tissue with skin was removed from the mouse immediately after it was sacrificed, and several drops of glycerol were pipetted on the surface of the tumor and the skin. Then, a piece of cover glass served to carefully mantle the tissue without introducing air bubbles in it. To image the distribution of LQDs in tumor tissues, we employed an HGM system [28]. The ultrafast laser source of our HGM system was a homebuilt femtosecond Cr:forsterite laser operating at 1230 nm with a 110 MHz repetition rate and a 100-fs pulse width. The laser beam was scanned by means of a galvanometer scanner (Olympus Fluoview 300, Germany), was guided to an upright microscope (Olympus BX-51, Germany), and was then focused onto samples by means of an IR water-immersion objective (Olympus LUMPlanFL/IR 60X/NA 0.9/Working distance 2 mm, Germany). The generated second and third harmonic signals were epi-collected by means of the same objective and were reflected in a dichroic mirror (Chroma Technology, VT), both of which served to guide the generated signals into different photomultiplier tubes (PMTs). In general, the experimental system allows for both the

collection of third harmonic generation (THG) image signals and the collection of second harmonic generation (SHG) image signals simultaneously [28]. Finally, the SHG and THG signals were reconstructed into  $512 \times 512$ -pixel images. The SHG microscopy can reveal the distribution and morphology of structured proteins such as collagen fibers [31]. The THG microscopy can depict the boundary of cells or organelles. In the previous study, we proved that LQDs can generate strong THG signals, which can serve as an excellent contrast agent in THG microscopy.

### 2.9. Determination of blood-vessel rupture with P-selectin expression

Fresh frozen tumor tissue was homogenized in a lysis buffer, kept overnight, and then centrifuged at  $7000 \times g$  for 30 min. After centrifugation to remove tissue debris, the protein contents of tissue homogenates were determined according to the Bradford method [32]. The supernatant with  $150 \mu\text{g}$  protein was dissolved in a sample buffer, was separated on a 5% SDS-PAGE, and was transferred to a polyvinylidene fluoride (PVDF) membrane. The PVDF membrane was further incubated with the anti-mouse P-selectin/CD62P primary antibody (1:1000), and was then incubated with the goat anti-mouse IgG (H+L) HRP-labeled secondary antibody (1:1000). For measuring the positive bands' optic density, the film was scanned by means of the BioSpectrum Imaging System (UVP LLC, Upland, CA).

### 2.10. Statistical analysis

Statistical analysis was performed with the STATVIEW (SAS Institute Inc, Cary, NC) statistical software, and we then calculated the difference between the cadmium concentration and the particle sizes by using ANOVA combined with post-hoc testing in comparisons between groups (UCA + LQDs, FUS + LQDs, and UCA + FUS + LQDs) and LQD injection only.

## 3. Results and discussion

### 3.1. Characterization of lipid-coated quantum dot nanoparticles (LQDs)

To formulate water-soluble quantum dots (QDs) for better bioavailability, we used a lipid-coating method in this study. Following the synthesized protocol, we prepared different sizes of LQDs using various amounts of DOPE-PEG2000 in a lipid mixture. Fig. 2A shows four groups of LQDs with sizes of  $30 \pm 6 \text{ nm}$ ,  $80 \pm 15 \text{ nm}$ ,  $130 \pm 25 \text{ nm}$ , and  $180 \pm 40 \text{ nm}$ , and the sizes were determined by means of a dynamic light-scattering particle analyzer. Each group of LQDs appeared as a composite spherical structure as shown in Fig. 2B, which is a transmission electron microscopy (TEM) picture. Apparently, the cholesterol-based lipid micelles can trap hydrophobic QDs and interact with QDs strongly enough to preserve the individuality of the LQDs. Fig. 2C shows the PL emission spectra for both free QDs and LQDs, and it indicates that, in general, there is no obvious change in the PL emission spectra from the pre-“lipid coating” stage to the post-“lipid coating” stage.

### 3.2. Enhancement of LQDs' extravasation by ultrasound sonication with microbubbles

To investigate the effects of both particle size and administration of FUS with UCA on the delivery of LQD nanoparticles in tumor tissues, we have studied four different sizes of LQD nanoparticles in *in vivo* experiments for five groups of treatment conditions: the control group, the LQD group, the UCA + LQD group, the FUS + LQD group, and the UCA + FUS + LQD group. The amount of cadmium extracted from LQDs deposited in the tumor tissues about 24 h after the injection of LQDs was quantitatively determined with graphite furnace atomic absorption spectrometry (GF-AAS). Fig. 3 shows that

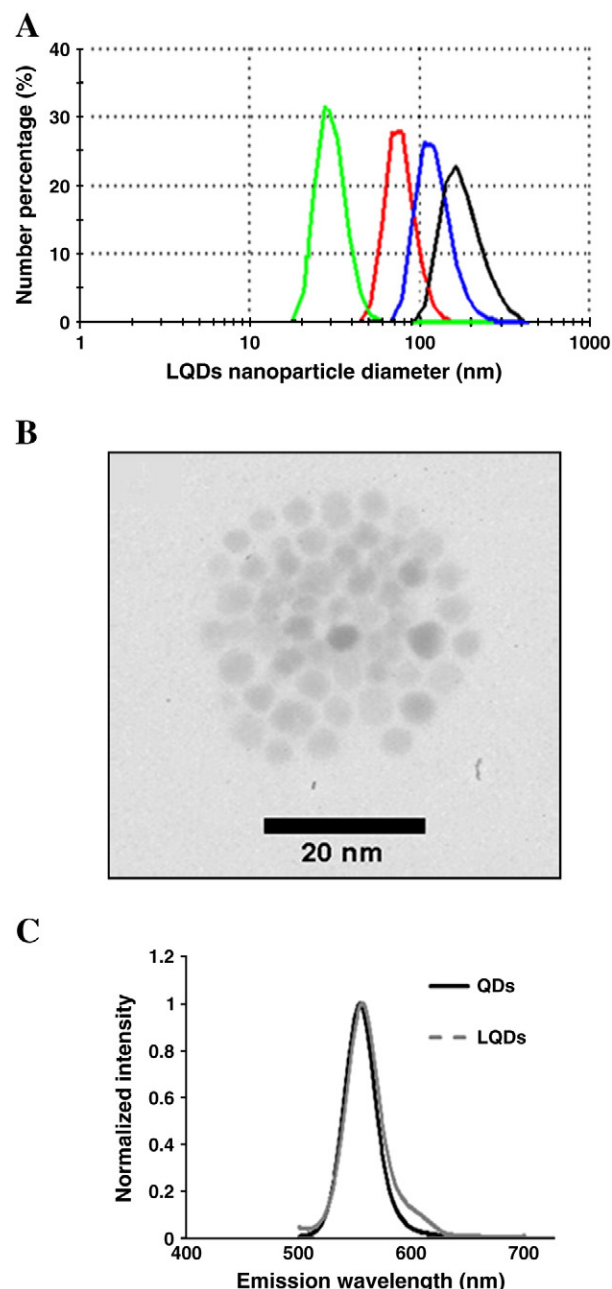


**Fig. 2.** Shows the characteristics of the LQD nanoparticles used in this study: (A) four sizes of LQDs ranging from  $30 \pm 6 \text{ nm}$ ,  $80 \pm 15 \text{ nm}$ , and  $130 \pm 25 \text{ nm}$  to  $180 \pm 40 \text{ nm}$ , measured by means of a dynamic light-scattering particle analyzer; (B) the LQDs' morphology, as represented by transmission electron microscopy; (C) the photoluminescence spectra of QDs and LQDs.

the amounts of cadmium deposited in the tumor tissues with UCA + FUS + LQDs were  $4.47 \pm 1.09$ ,  $2.27 \pm 0.26$ ,  $0.99 \pm 0.18$ , and  $0.82 \pm 0.28$  ( $\mu\text{g Cd}/(\text{g tumor})$ ) for 30, 80, 130, and 180 nm of LQDs, respectively; as compared with LQD injection only, whose corresponding amounts were  $1.12 \pm 0.33$ ,  $0.75 \pm 0.13$ ,  $0.26 \pm 0.22$ , and  $0.34 \pm 0.04$  ( $\mu\text{g Cd}/(\text{g tumor})$ ). In addition, Fig. 3 displays the percentage of the injected dose of LQDs per gram of tumor tissue (% ID/g tumor)). The values of the % ID/g tumor) in the tumor tissue in the UCA + FUS + LQD group were  $30.55 \pm 7.44$ ,  $15.51 \pm 1.80$ ,  $6.77 \pm 1.29$ , and  $5.61 \pm 1.90$  for 30, 80, 130, and 180 nm of LQDs, respectively; and the corresponding values in LQD group were  $7.65 \pm 2.23$ ,  $5.16 \pm 0.90$ ,  $1.80 \pm 1.53$ , and  $2.35 \pm 0.34$ . The amount of LQDs delivered into the tumor tissues for FUS sonication in the presence of microbubbles was much greater than those for other conditions (control, LQDs, UCA + LQDs, and FUS +

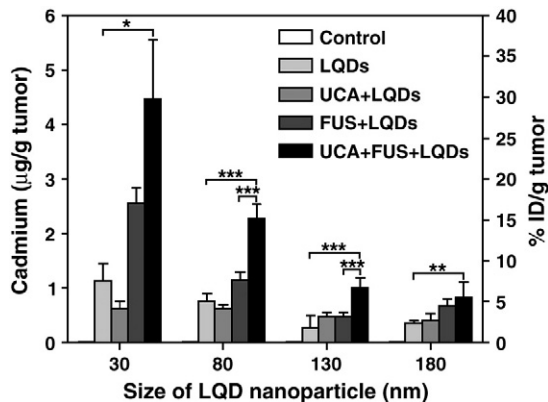


**Fig. 3.** Shows the amounts of Cd extracted from four different sizes of LQD nanoparticles deposited in the tumor tissues with five different treatment conditions: control, LQDs, UCA + LQDs, FUS + LQDs, UCA + FUS + LQDs. The figure also shows the percentage values of the injected dose of LQD nanoparticles per gram of tumor tissues (for each condition,  $n \geq 3$ ; and mean plus SD.) Statistical significance compared with LQD injections only; \*\*\* $P < 0.0001$ , \*\* $P \leq 0.0005$ , and \* $P < 0.005$ .

LQDs), and the difference is statistically significant (\*\* $P < 0.0001$ , \*\* $P \leq 0.0005$ , and \* $P < 0.005$ ) for all particle sizes. In addition, smaller LQDs exhibited higher delivery efficiency than larger LQDs, and the amount of cadmium extracted from the tumor tissues for 30 nm LQDs was about 2-, 4.5-, or 5.5-folds greater than those for 80, 130, or 180 nm of LQDs. A smaller LQD would exhibit higher permeability, and this phenomenon exhibited itself also in non-sonication cases.

The results of Fig. 3 also show that there is statistical significance between FUS and FUS/UCA groups for 80 and 130 nm, but not for 30 and 180 nm. This indicates that the vascular rupture caused by FUS/UCA has a higher delivery enhancement for the medium size of LQD nanoparticles between 80 and 130 nm than other particle sizes.

### 3.3. Optical imaging analysis of LQDs' release enhanced by ultrasound sonication with microbubbles

To further study the extravasation of LQDs from vasculature to tumor tissues, we employed photoluminescence (PL) spectrometry, which enabled us specifically to analyze the emission spectrum of LQDs, and we employed harmonic generation microscopy (HGM), which enabled us specifically to map the distribution of LQDs in the tumor tissue. Fig. 4A shows the representative PL spectra for the injections of different sizes of LQDs with or without FUS sonication in the presence of microbubbles. To demonstrate that vascular permeability can be enhanced through the application of ultrasound sonication to microbubbles, we performed PL spectra of tissue sections. As a control, we first measured the background autofluorescence spectrum of a tissue sectioned from a mouse tumor (without the injection of LQDs or ultrasound sonication). The detected counts of spectral intensity were typically from 8000 to 15,000 in the emission-wavelength range of LQDs (540 to 590 nm), (green curves in Fig. 4A). Under the same slit width and integration time, we then measured the spectra of tissues sectioned from mice injected with 30 nm, 80 nm, 130 nm, and 180 nm of LQDs, separately (black curves in Fig. 4A). In each case, the FUS sonication on tumor tissues could enhance the PL intensity of tumor tissue sections (blue curves in Fig. 4A). The injection of microbubbles before FUS sonication could further enhance the PL intensity (red curves in Fig. 4A), a result indicating that there was more extravasation of LQDs from blood vessels into the tumor tissues. Fig. 4B displays the spike of the major characteristic emission wavelength (from 553 to 557 nm) by different treatment groups. The results support the assertion that the vascular permeability for LQDs can be greatly enhanced by FUS sonication in the presence of microbubbles. For this PL system, each count was equal to ten photons and its value represents the intensity calculation. The

emission intensity from the FUS sonication groups was higher than that from the non-sonication groups for all different sizes of LQDs, especially for smaller LQDs.

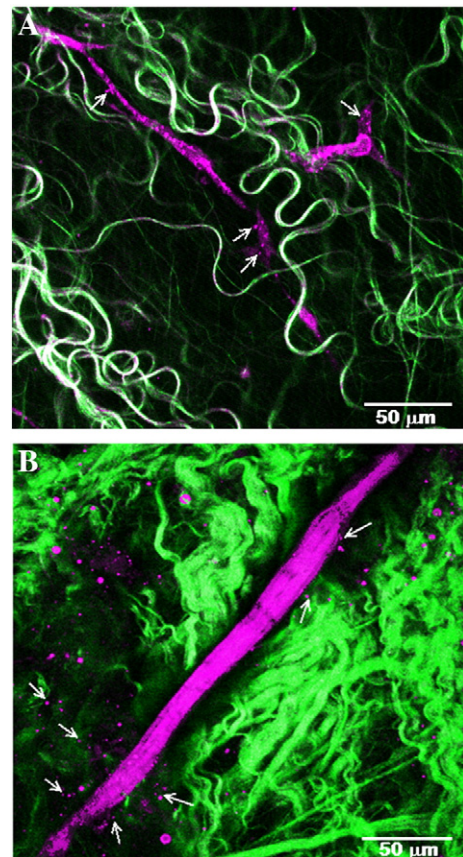
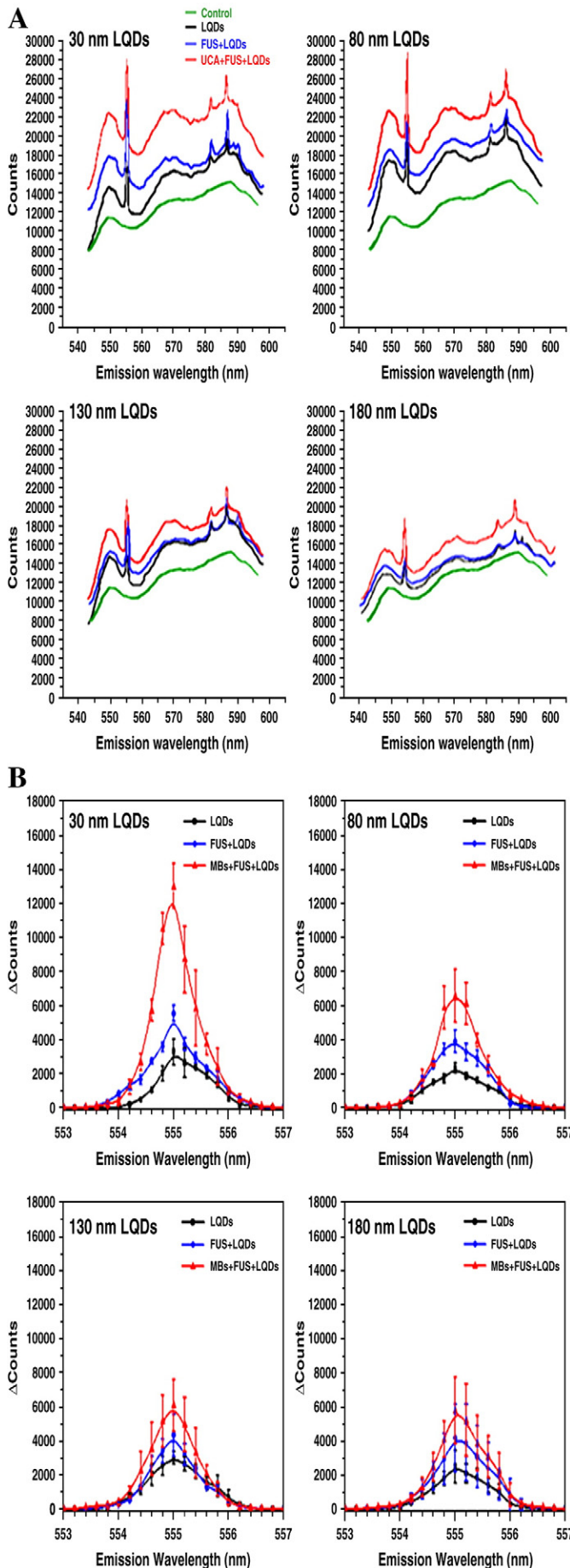
To obtain microscopic evidence, we further used harmonic generation microscopy (HGM), which yields images depicting the deposition of extravasated LQDs in tumor tissues. To generate strong third harmonic generation (THG) signals from nanoparticles, we used 130 nm LQDs for this imaging, and Fig. 5 is an HGM for without- and with-FUS sonication in the presence of microbubbles. Second harmonic generation (SHG) images (green) represent the network of collagen fibers, and the strong THG (magenta) signal depicts tumor vasculature and the distribution of LQDs. This figure indicates that HGM can clearly identify the deposition of the extravasated LQDs in the tumor tissues and the tissue texture.

Fig. 5, dealing with harmonic generation microscopy (HGM), shows the deposition of LQDs in the sonicated tumor tissues. Because the THG signals of LQDs are much stronger than those of background tissues, the pronounced magenta spots certainly came from the LQDs. This finding indicates that LQDs constitute a good optical surrogate marker to track nanodrug deposition in tumor tissues. The slice thickness of each microscopic image was 1.0  $\mu\text{m}$ , meaning that the same figure shows all of the LQDs deposited within this region. A blood vessel lying along the diagonal of the figure is full of LQDs. Since the orientation of the vessel was not parallel to the imaging plane, the widths of the vessel varied. This region exhibited strong THG signals, which could be from the blood vessel combined with the diffused LQDs adjacent to the vessel. Dots of the deposited LQDs were perhaps diffused from this vessel or surrounding vessels (above or beneath this plane) because of the constraints of the interstitium and the "FUS sonication"-induced changes in the tumor microenvironment. The green color represents collagen networks, and the hollow area represents a location full of cells. The tissue structure and the distribution of LQDs indicate that the tissue texture and the interstitium could limit the delivery of LQDs from blood vessels into tumor tissues.

For sub-wavelength nanoparticles, the yield for third harmonic generation (THG) is proportional to their volume [28]. Therefore, in order to obtain a detectable THG contrast of LQDs and keep the size as small as possible, we selected 130-nm LQDs for the demonstration of the microscopic images showing the extravasation of nanoparticles in the tumor tissues. Comparing Fig. 4A with Fig. 3, we can find that the enhancement factor measured by PL spectra is obviously smaller than that by AAS. This discrepancy of enhancement factors between PL spectra and AAS may originate from a) the interference of the high background autofluorescence in the tumor tissues, b) the photo bleaching of LQDs, and c) locally inhomogeneous distribution of LQDs [28,31]. As the spike of the major characteristic emission wavelength (Fig. 4B) is taken into consideration, the discrepancy of enhancement factors can be reduced. It indicates that the spike of major characteristic emission is a better indicator than the entire PL spectra to show the relative quantity of LQD nanoparticles in the tissues.

### 3.4. Blood vessel rupture determined by P-selectin expression

To study the vascular destruction in the sonicated tumor caused by FUS sonication in the presence of microbubbles, we used endothelial cell P-selectin protein expression. P-selectin protein expression was a biochemical marker that we used to determine whether blood vessels in the tumor tissue of the mice were ruptured or not after FUS sonication in the presence of microbubbles [33,34]. We used 130 nm of LQDs for this study, and Fig. 6 shows that P-selectin appeared as a major band at approximately 140 kDa and that its intensity value for ultrasound-mediated UCA (the UCA + FUS + LQD group) disruption was about 4.5-fold greater than the other conditions (control, LQDs, and FUS + LQDs). These findings indicate that ultrasound-mediated microbubble oscillation and cavitation induce significant vascular



**Fig. 5.** Concerns the harmonic generation microscopy (HGM) attributable to tumor tissues taken from mice sacrificed (A) about 1 h after an LQD injection only, and (B) about 1 h after an LQD injection (preceded by both a UCA injection and FUS sonication). The HGM shows the deposition and the distribution of LQDs (white arrows) and the tissue texture. It validates the assertion that there was a triggered release of LQDs from vasculature to tumor tissue after UCA injection plus FUS sonication. The magenta color represents LQDs (which constituted the third harmonic generation (THG) contrast agent), and the green color represents the collagen networks.

rupture ( $***P<0.0001$ ). However, some studies [35,36] show that the increase of P-selectin expression can cause inflammatory responses and might be a stimulus to tumor angiogenesis. This indicates that ultrasound-mediated microbubble destruction can enhance the delivery of nanoparticle drugs to sonicated tumors while perhaps also promoting tumor growth. Further research should investigate the resulting effects that the counteractions of ultrasound-mediated microbubble destruction can have on tumor treatment.

We implanted T-type thermocouples in intratumor locations to measure the temperature responses for the 120 s of pulsed FUS sonication at room temperature. The maximum temperature rise was about  $2.5^{\circ}\text{C}$  for pulsed FUS alone and was about  $4.1^{\circ}\text{C}$  for pulsed FUS plus UCA, and the total temperature rise durations were about 200 s. The temperature responses indicate that, in general, the 1.2-MPa pulsed FUS sonication can result in a brief low-temperature hyperthermia effect on the sonicated tumor tissues for both with and without UCA injection. Both Figs. 3 and 4 show that short-time pulsed FUS sonication without injection of UCA had some effect on the

**Fig. 4.** (A) Shows photoluminescence (PL) emission spectra of tumor tissues for injection of different sizes of LQD nanoparticles in different treatment conditions: control, LQDs only, FUS plus LQDs, and UCA plus FUS and LQDs; (B) shows the spike of the major characteristic emission wavelength from 553 to 557 nm.

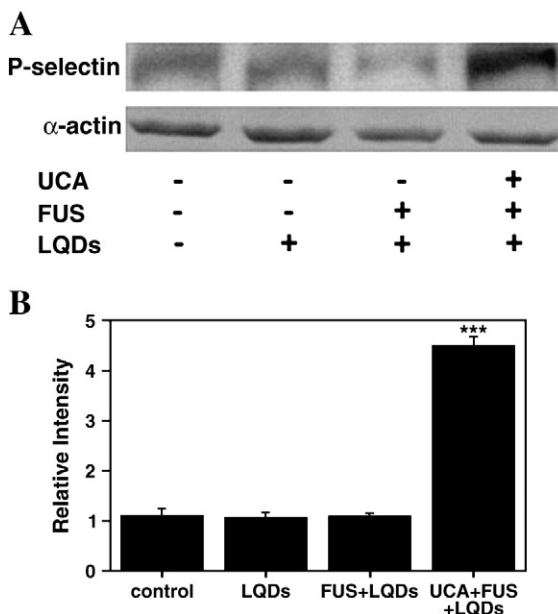


**Fig. 6.** Shows the western blotting analysis of sonicated tumor tissues and its P-selectin expression for tumor endothelial cells. The following conditions are studied: control, LQD injections only, FUS sonication plus LQD injections, and UCA injections plus FUS sonication plus LQD injections. Tumor tissue lysates ( $2\ \mu\text{g}/\text{lane}$ ) were performed on a 5% SDS-PAGE and were immunoblotted with rmP-selectin/CD62P antibodies or anti- $\alpha$ -actin. The band for the UCA plus FUS plus LQDs exhibited a strong expression of P-selectin. Actin functioned as a control for protein loading. (For each condition,  $n \geq 3$ ; and mean plus SD). Statistical significance compared with LQD injection only; \*\*\* $P < 0.0001$ .

delivery of LQD nanoparticles, and this effect could reflect both the brief thermal and mechanical actions of 1.2-MPa pressure on the sonicated tumor tissues, but the effect was not significant. In addition, previous studies [7,8] show that hyperthermia could be employed to increase the nanodrug delivery to the tumor tissue, and ultrasound energy can be focused on the target region to raise and maintain the local tissue temperature at a desired level. This indicates that after the local blood vessels in the sonicated tumor are disrupted with pulsed FUS and microbubbles, we may then employ continuous FUS to generate local hyperthermia to further boost the nanoparticle delivery into the tumor tissues.

In order to investigate the influence of individual treatment procedure on the accumulation of LQDs in the tumor tissues, we arranged the injection of LQDs always at the last step of treatment in this study and sacrificed the animals about 24 h after the treatment. By comparing the amounts of LQDs deposited in the tumor tissues, we could identify the individual influence of UCA, FUS, and UCA + FUS on the nanoparticle delivery for the following 24 h. In contrast, Bekeredjian et al. [37] used Evans blue (about 1000 Da) as an indicator to demonstrate that ultrasound-mediated microbubble destruction could enhance the accumulation of Evans blue in the sonicated tumor tissues for the following 30 min after sonication. They showed that the injection of Evans blue prior to both microbubble injection and ultrasound sonication could dramatically enhance the short-time accumulation of Evans blue in the sonicated tumor tissues. This indicates that the interaction between ultrasound waves and Evans blue in the presence of microbubbles is a major factor for a short-time accumulation. With the LQD solution injected first, intrinsically, the mechanical action of FUS sonication and/or the interaction of FUS beam with microbubbles can further boost the delivery of nanoparticles into the tumor tissues during the sonication period. Furthermore, the short-time temperature rise during pulsed FUS sonication in the presence of UCA may have similar effect to increase the accumulation of LQD nanoparticles in the tumors. Hence, it is worthwhile to further study the influence of treatment sequence

with LQD injection first on the long-time accumulation of nanoparticles in sonicated tumor tissues.

As shown in Fig. 3, the amount of cadmium extracted from the tumor tissues in the UCA + LQD group was smaller than that in the LQD group when the size of injected LQD nanoparticles was 30 or 80 nm, while the amount of extracted cadmium in the UCA + LQD group was greater when the size of injected LQDs was 130 or 180 nm. For the case with 30-nm LQDs, the difference of extracted cadmium between the two groups is noticeable, and this may be due to the quantity of PEG-lipid used in making LQD nanoparticles and the properties of microbubbles. The UCA (SonoVue®) used in this study was phospholipid-coated microbubbles with a mean diameter of about 2.5  $\mu\text{m}$ , a bubble concentration of  $2\text{--}5 \times 10^8$  bubbles/mL, and an injected dose of  $30\ \mu\text{L}/\text{kg}$ . After being injected into the blood vessel, the microbubbles will completely dissolve in bloodstream within several minutes. The negatively charged microbubbles may affect the delivery of cationic LQDs into tumor tissues, especially for 30-nm nanoparticles, which contain a high percentage of PEG-lipid (10%) [38]. Further study may be required to evaluate the effect of microbubbles on the delivery of nanoparticles into tumor tissues in order to choose suitable types of UCAs to match the formulae of the carrier system for a drug.

#### 4. Conclusion

The *in vivo* experiments demonstrate that FUS sonication under the presence of microbubbles could significantly enhance the delivery of LQD nanoparticles into tumor tissues in a mouse tumor model. Immunoblotting analysis further indicates that FUS sonication could induce the destruction of microbubbles and could, thus, cause the rupture of blood vessels' walls, which would increase vascular permeability and which would, in turn, elevate the amount of LQDs deposited in sonicated tumor tissues. In addition, FUS sonication might change the tissue microenvironment and facilitate the delivery of LQDs to a region farther away from the blood vessels, while the constraints of tissue texture, the interstitium, and the fluid pressure limit the delivery distance from blood vessels.

#### Acknowledgements

This work was supported by the National Health Research Institutes Grant (no. NHRI: 96A1-MEPP13-014); and the National Science Council of Taiwan (no. NSC: 97-2120-M-002-017). We are particularly grateful to Dr. Ja-Liang Lin, RN Dan-Tzu Lin-Tan, and Dr. Pao-Hsien Chu for their assistance and facilities in helping this manuscript. The HGM imaging is supported by the National Taiwan University Research Center for Medical Excellence.

#### References

- [1] G. Bergers, L.E. Benjamin, Tumorigenesis and the angiogenic switch, *Nat. Rev. Cancer* 3 (6) (2003) 401–410.
- [2] R.K. Jain, 1995 Whitaker lecture: delivery of molecules, particles, and cells to solid tumors, *Ann. Biomed. Eng.* 24 (4) (1996) 457–473.
- [3] Y. Boucher, L.T. Baxter, R.K. Jain, Interstitial pressure gradients in tissue-isolated and subcutaneous tumors: implications for therapy, *Cancer Res.* 50 (15) (1990) 4478–4484.
- [4] N. Rapoport, W.G. Pitt, H. Sun, J.L. Nelson, Drug delivery in polymeric micelles: from *in vitro* to *in vivo*, *J. Control. Release* 91 (1) (2003) 85–95.
- [5] C.L. Peng, P.S. Lai, F.H. Lin, Y.H. Wu, M.J. Shieh, Dual chemotherapy and photodynamic therapy in an HT-29 human colon cancer xenograft model using SN-38-loaded chlorine-core block copolymer micelles, *Biomaterials* 30 (21) (2009) 3614–3625.
- [6] M. Leunig, A.E. Goetz, M. Delliam, G. Zetterer, F. Gamarra, R.K. Jain, K. Messmer, Interstitial fluid pressure in solid tumors following hyperthermia: possible correlation with therapeutic response, *Cancer Res.* 52 (2) (1992) 487–490.
- [7] G. Kong, R.D. Braun, M.W. Dewhirst, Hyperthermia enables tumor-specific nanoparticle delivery: effect of particle size, *Cancer Res.* 60 (12) (2000) 4440–4445.
- [8] M.R. Dreher, W. Liu, C.R. Michelich, M.W. Dewhirst, A. Chilkoti, Thermal cycling enhances the accumulation of a temperature-sensitive biopolymer in solid tumors, *Cancer Res.* 67 (9) (2007) 4418–4424.

- [9] R.K. Schlicher, H. Radhakrishna, T.P. Tolentino, R.P. Apkarian, V. Zarnitsyn, M.R. Prausnitz, Mechanism of intracellular delivery by acoustic cavitation, *Ultrasound Med. Biol.* 32 (6) (2006) 915–924.
- [10] G.A. Hussein, W.G. Pitt, The use of ultrasound and micelles in cancer treatment, *J. Nanosci. Nanotechnol.* 8 (5) (2008) 2205–2215.
- [11] R.J. Price, D.M. Skyba, S. Kaul, T.C. Skalak, Delivery of colloidal particles and red blood cells to tissue through microvessel ruptures created by targeted microbubble destruction with ultrasound, *Circulation* 98 (13) (1998) 1264–1267.
- [12] N.Y. Rapoport, A.M. Kennedy, J.E. Shea, C.L. Scaife, K.H. Nam, Controlled and targeted tumor chemotherapy by ultrasound-activated nanoemulsions/microbubbles, *J. Control. Release* 138 (3) (2009) 268–276.
- [13] D.B. Ellegala, H. Leong-Poi, J.E. Carpenter, A.L. Klibanov, S. Kaul, M.E. Shaffrey, J. Sklenar, J.R. Lindner, Imaging tumor angiogenesis with contrast ultrasound and microbubbles targeted to  $\alpha_1\beta_3$ , *Circulation* 108 (3) (2003) 336–341.
- [14] P.A. Netti, L.T. Baxter, Y. Boucher, R. Skalak, R.K. Jain, Time-dependent behaviour of interstitial fluid pressure in solid tumors: implications for drug delivery, *Cancer Res.* 55 (22) (1995) 5451–5458.
- [15] A.V. Salnikov, V.V. Inversen, M. Koisti, C. Sundberg, L. Johansson, L.B. Stuhr, M. Sjoquist, H. Ahlstrom, R.K. Reed, K. Rubin, Lowering of tumor interstitial fluid pressure specifically augments efficacy of chemotherapy, *FASEB J.* 17 (12) (2003) 1756–1758.
- [16] M.J. Shieh, C.L. Peng, P.J. Lou, C.H. Chiu, T.Y. Tsai, C.Y. Hsu, C.Y. Yeh, P.S. Lai, Non-toxic phototriggered gene transfection by PAMAM-porphyrin conjugates, *J. Control. Release* 129 (3) (2008) 200–206.
- [17] J.B. Wolinsky, M.W. Grinstaff, Therapeutic and diagnostic applications of dendrimers for cancer treatment, *Adv. Drug Deliv. Rev.* 60 (9) (2008) 1037–1055.
- [18] A.S. Mikhail, C. Allen, Block copolymer micelles for delivery of cancer therapy: transport at the whole body, tissue and cellular levels, *J. Control. Release* 138 (3) (2009) 214–223.
- [19] M.R. Dreher, W. Liu, C.R. Michelich, M.W. Dewhirst, F. Yuan, A. Chikotli, Tumor vascular permeability, accumulation, and penetration of macromolecular drug carriers, *J. Natl. Cancer Inst.* 98 (5) (2006) 335–344.
- [20] Y. Liu, H. Miyoshi, M. Nakamura, Nanomedicine for drug delivery and imaging: a promising avenue for cancer therapy and diagnosis using targeted functional nanoparticles, *Int. J. Cancer* 120 (2007) 2527–2537.
- [21] R. Jain, P. Dandekar, V. Patravale, Diagnostic nanocarriers for sentinel lymph node imaging, *J. Control. Release* 138 (2) (2009) 90–102.
- [22] J.E. Schroeder, I. Shweky, H. Shmeeda, U. Banin, A. Gabizon, Folate-mediated tumor cell uptake of quantum dots entrapped in lipid nanoparticles, *J. Control. Release* 124 (1–2) (2007) 28–34.
- [23] M.N. Rhyner, A.M. Smith, X. Gao, H. Mao, L. Yang, S. Nie, Quantum dots and multifunctional nanoparticles: new contrast agents for tumor imaging, *Nanomedicine* 1 (2) (2006) 209–217.
- [24] G.D. Bothun, A.E. Rabideau, M.A. Stoner, Hepatoma cell uptake of cationic multi fluorescent quantum dot liposomes, *J. Phys. Chem. B* 113 (22) (2009) 7725–7728.
- [25] D.R. Larson, W.R. Zipfel, R.M. Williams, S.W. Clark, M.P. Bruchez, F.W. Wise, W.W. Webb, Water-soluble quantum dots for multiphoton fluorescence imaging in vivo, *Science* 300 (5624) (2003) 1434–1436.
- [26] B. Duerret, P. Skourides, D.J. Norris, V. Noireaux, A.H. Brivanlou, A. Libchaber, In vivo imaging of quantum dots encapsulated in phospholipid micelles, *Science* 298 (5599) (2002) 1759–1762.
- [27] H. Zhang, D. Yee, C. Wang, Quantum dots for cancer diagnosis and therapy: biological and clinical perspectives, *Nanomedicine* 3 (1) (2008) 83–91.
- [28] C.F. Chang, C.Y. Chen, F.H. Chang, S.P. Tai, C.Y. Chen, C.H. Yu, Y.B. Tseng, I.S. Liu, W.F. Su, C.K. Sun, Quantum dots for cancer diagnosis and therapy: biological and clinical perspectives, *Opt. Express* 16 (13) (2008) 9534–9548.
- [29] S.A. Majetich, A.C. Carter, Surface effects on the optical-properties of cadmium selenide quantum dots, *J. Phys. Chem.* 97 (34) (1993) 8727–8737.
- [30] O. Carion, B. Mahler, T. Pons, B. Dubertret, Synthesis, encapsulation, purification and coupling of single quantum dots in phospholipid micelles for their use in cellular and in vivo imaging, *Nat. Protocols* 2 (10) (2007) 2383–2390.
- [31] T.M. Liu, Y.W. Lee, C.F. Chang, S.C. Yeh, C.H. Wang, S.W. Chu, C.K. Sun, Imaging polyhedral inclusion bodies of nuclear polyhedrosis viruses with second harmonic generation microscopy, *Opt. Express* 16 (8) (2008) 5602–5608.
- [32] M.M. Bradford, A rapid and sensitive methods for quantification of microgram quantities of protein utilizing the principle for protein-dye binding, *Anal. Biochem.* 7 (72) (1976) 248–254.
- [33] J.J. Rychak, J.R. Lindner, K. Ley, A.L. Klibanov, Deformable gas-filled microbubbles targeted to P-selectin, *J. Control. Release* 114 (3) (2006) 288–299.
- [34] J.J. Rychak, A.L. Klibanov, J.A. Hossack, Acoustic radiation force enhances targeted delivery of ultrasound contrast microbubbles: in vitro verification, *IEEE Trans. Ultrason. Ferroelectr. Freq. Control* 52 (3) (2005) 421–433.
- [35] D.W. Hartwell, C.E. Butterfield, P.S. Frenette, B.M. Kenyon, R.O. Hynes, J. Folkman, D.D. Wagner, Angiogenesis in P- and E-selectin-deficient mice, *Microcirculation* 5 (1998) 173–178.
- [36] D. Hanahan, J. Folkman, Patterns and emerging mechanisms of the angiogenic switch during tumorigenesis, *Cell* 86 (1996) 353–364.
- [37] R. Bekerdjian, R.D. Kroll, E. Fein, S. Tinkov, C. Coester, G. Winter, H.A. Katus, H. Kulaksiz, Ultrasound targeted microbubble destruction increases capillary permeability in hepatomas, *Ultrasound Med. Biol.* 33 (10) (2007) 1592–1598.
- [38] N.G. Fisher, J.P. Christiansen, A. Klibanov, R.P. Taylor, S. Kaul, J.R. Lindner, Influence of microbubble surface charge on capillary transit and myocardial contrast enhancement, *J. Am. Coll. Cardiol.* 26 (2002) 1340–1347.